Optimal control

Shape optimization of a layer by layer mechanical constraint for additive manufacturing

Optimisation de forme pour une contrainte mécanique associée aux procédés de fabrication additive

Grégoire Allaire [a], Charles Dapogny [b], Alexis Faure [c], Georgios Michailidis [c]

[a] *Centre de mathématiques appliquées, École polytechnique, CNRS, Université Paris-Saclay, 91128 Palaiseau, France*
[b] *Laboratoire Jean-Kuntzmann, CNRS, Université Grenoble-Alpes, BP 53, 38041 Grenoble cedex 9, France*
[c] *SIMaP, Université Grenoble-Alpes, BP 53, 38041 Grenoble cedex 9, France*

A R T I C L E   I N F O

A B S T R A C T

The purpose of this article is to introduce a new functional of the domain, to be used in shape optimization problems as a means to enforce the constructibility of shapes by additive manufacturing processes. This functional aggregates the self-weights of all the intermediate structures of the shape appearing in the course of its layer-by-layer assembly. Its mathematical analysis is performed and an algorithm is proposed to accelerate the significant computational effort entailed by the implementation of these ideas. Eventually, a numerical validation and a concrete example are discussed.

© 2017 Académie des sciences. Published by Elsevier Masson SAS. This is an open access article under the CC BY-NC-ND license (http://creativecommons.org/licenses/by-nc-nd/4.0/).

R É S U M É

Nous introduisons dans cet article une nouvelle fonctionnelle dépendant du domaine qui, utilisée comme contrainte dans un problème d'optimisation de forme, impose la constructibilité par les procédés de fabrication additive. Cette fonctionnelle agrège les poids propres de toutes les structures intermédiaires de la forme mises en jeu au cours du processus d'assemblage par strates. Après son analyse mathématique, nous proposons un algorithme pour accélérer significativement les calculs coûteux entraînés par l'implémentation de ces idées. Une validation numérique ainsi qu'un exemple concret sont enfin présentés.

© 2017 Académie des sciences. Published by Elsevier Masson SAS. This is an open access article under the CC BY-NC-ND license (http://creativecommons.org/licenses/by-nc-nd/4.0/).
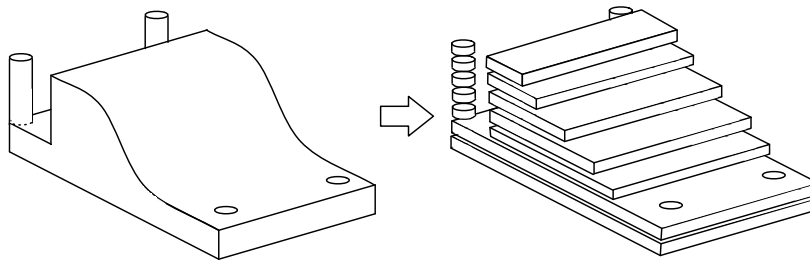
Fig. 1. Rough sketch of the slicing procedure, initiating any additive manufacturing process.

1. Introduction

The additive manufacturing technologies have demonstrated a unique potential in realizing structures with a high degree of complexity, thereby allowing one to process almost directly the designs predicted by shape and topology optimization algorithms [12]. These breakthroughs come along with new opportunities, and with new challenges – see [7] for a detailed and comprehensive overview of both, and the references therein.

To summarize its main features in a few words, additive manufacturing is a common label for quite different methodologies, which share the fact that the construction process starts with a slicing procedure: the Computer-Aided Design (CAD) model for the input shape (which is often supplied by means of a mesh under the popular STL format [25]) is converted into a series of two-dimensional layers (see Fig. 1).

Thence, these layers are assembled individually, one above the other, according to the selected technology. As far as these technologies are concerned, two important categories are the following:

– material extrusion methods, such as Fused Filament Fabrication (FFF), act by selectively extruding the molten material through a nozzle; such methods are typically used to process plastic (ABS);
– powder bed fusion methods (such as Selective Laser Sintering, or Electron Beam Melting) are on the contrary used to process metals; at the beginning of the construction of each layer, metallic powder is spread within the build chamber and a laser (or an electron beam) is used to bind the grains together.

These technologies show competing features in terms of cost, speed, accuracy... and also in terms of the restrictions they impose on the manufacturing process and the constructed shape. Beyond their differences, one challenge is faced by all additive manufacturing technologies, that of building shapes showing large *overhangs*, i.e. regions hanging over void (or powder) without sufficient support from the lower structure.

– In the case of material extrusion methods, parts of the boundary showing large overhangs cannot be produced as is, since this demands depositing material on void.
– In the case of powder bed fusion methods, the rapid melting then solidification of the material induces large thermal variations in the structure; this creates residual stresses, and causes the structure to warp. This phenomenon is all the more likely to occur in regions that are unanchored to the lower structure (in particular, overhanging regions); see [19]. Another source of difficulties in the assembly of overhanging regions lies in that the fused material may drip between the unfused powder of the lower structure, thus leaving the processed boundary with rough patches [5].

One way to cope with the presence of overhangs is to erect scaffolds (or supports) at the same time as the shape is constructed, with the purpose of anchoring the overhanging regions [8]. This scaffold structure has to be removed manually at the end of the process, which is cumbersome and time-consuming. Another way is to constrain the presence of overhangs in the formulation of the shape optimization problem guiding the design of the shape. Hitherto, ad hoc criteria, based on a minimum angle between the structural boundary and the horizontal directions, have been used to tackle this issue [11,17, 18].

The present article is devoted to the modeling and the mathematical analysis of a new mechanical constraint for the optimization of shapes that are processed by an additive manufacturing method. Several variants of this constraint, and various numerical examples and discussions of engineering applications will be presented in a forthcoming article [4]. Under the simplifying assumption that the components of one single layer of material are built simultaneously during the manufacturing process, we introduce a new constraint functional for shape optimization problems, which appraises the constructibility of shapes at each stage of their assembly. In particular, overhang constraints are naturally addressed by this formulation, which appeals to their mechanical origin. To achieve our purpose, in the setting of the optimization problem, we distinguish the mechanical situation where the final shape Ω is utilized, on which the optimization criterion is based, and that where Ω (and all the successive, intermediate structures) is under construction, which guides the definition of our constraint functional. Our first main result is to provide a shape derivative for this new constraint functional (see

Theorem 3.1), which is not a completely standard matter since the upper boundaries of the intermediate shapes are not subject to optimization, being dictated by the additive manufacturing process.

Our second main result is an acceleration method for the computation of our new constraint functional and for that of its shape derivative. Indeed, their expressions involve mechanical problems posed on all the intermediate structures of the considered shape, the number of which is precisely the number of layers in the additive manufacturing process (typically of the order of a few hundreds). Therefore, these evaluations are quite costly in numerical practice. Our idea is to interpolate, with piecewise affine functions of the height, the values of the functional and of its derivative, thus relying on the derivatives of the mechanical solutions with respect to the height of the intermediate structures.

This article is organized as follows. In Section 2, we introduce our shape optimization problem. In Section 3, we describe the mechanical context in which shapes are constructed, we formulate our new manufacturing constraint and we prove our first main mathematical result, Theorem 3.1, concerning its shape derivative. As we have mentioned, the resulting functional of the domain and its shape derivative are costly to evaluate in practice. Thus, in Section 4 we propose an interpolation method for accelerating significantly these calculations. For this purpose, we introduce a variant of the Hadamard method of shape deformations where only the upper horizontal boundary of the intermediate structures is allowed to vary, while the rest of the boundary is fixed. In this setting, first-order Taylor approximations of the mechanical performances of the intermediate shapes can be computed in terms of the height. Eventually, a numerical validation of our acceleration process and an optimization example are provided in Section 5.

2. Presentation of the shape optimization problem

A shape is a bounded, regular domain $\Omega \subset \mathbb{R}^d$, $d = 2, 3$, filled with a linear elastic material with Hooke's law A. In the context of its final utilization, Ω is clamped on a subset $\Gamma_D \subset \partial\Omega$, and it is submitted to surface loads $f \in L^2(\Gamma_N)^d$ applied on a region Γ_N of $\partial\Omega$ disjoint from Γ_D; the remaining part of the boundary $\Gamma := \partial\Omega \setminus (\overline{\Gamma_D} \cup \overline{\Gamma_N})$ is traction-free. The elastic displacement u_Ω^m is the unique solution in $H^1_{\Gamma_D}(\Omega)^d := \{u \in H^1(\Omega)^d, \ u = 0 \text{ on } \Gamma_D\}$ to the *mechanical* system:

$$\begin{cases} -\mathrm{div}(Ae(u_\Omega^m)) = 0 & \text{in } \Omega, \\ u_\Omega^m = 0 & \text{on } \Gamma_D, \\ Ae(u_\Omega^m)n = 0 & \text{on } \Gamma, \\ Ae(u_\Omega^m)n = f & \text{on } \Gamma_N. \end{cases} \tag{1}$$

For simplicity, the objective $J(\Omega)$ driving the optimization problem is the *compliance*:

$$J(\Omega) = \int_\Omega Ae(u_\Omega^m) : e(u_\Omega^m) \, \mathrm{d}x = \int_{\Gamma_N} f \cdot u_\Omega^m \, \mathrm{d}s. \tag{2}$$

Our optimization problem then reads:

$$\min_{\Omega \in \mathcal{U}_{\mathrm{ad}}} J(\Omega), \text{ such that } P(\Omega) \leq \alpha. \tag{3}$$

In (3), $\mathcal{U}_{\mathrm{ad}}$ is a set of admissible shapes Ω, which are assumed to be of class $\mathcal{C}^\infty$ for simplicity, and whose boundaries enclose the non-optimizable regions Γ_D, Γ_N and Γ_0 (the latter is defined in Section 3 below), i.e.

$$\mathcal{U}_{\mathrm{ad}} = \left\{ \Omega \subset \mathbb{R}^d \text{ is open, bounded, and of class } \mathcal{C}^\infty, \ \Gamma_D \cup \Gamma_N \cup \Gamma_0 \subset \partial\Omega \right\},$$

$P(\Omega)$ is our new constraint functional, whose definition and properties are discussed in the next sections, and α is a tolerance threshold. In practice, so that (3) be physically relevant, other constraints (e.g., on the volume $\mathrm{Vol}(\Omega)$ of shapes) may be added, which we omit for the mathematical analysis; see Section 5.

Most popular optimization algorithms for the numerical resolution of (3) rely on the derivatives of $J(\Omega)$ and $P(\Omega)$ with respect to the domain; these are understood in the framework of Hadamard's method (see, e.g., [1,15,20,22,24]): variations of a shape Ω are considered under the form:

$$\Omega_\theta := (\mathrm{Id} + \theta)(\Omega), \ \theta \in W^{1,\infty}(\mathbb{R}^d, \mathbb{R}^d), \ ||\theta||_{W^{1,\infty}(\mathbb{R}^d,\mathbb{R}^d)} < 1.$$

A generic function $F(\Omega)$ of the domain is then *shape differentiable* if the underlying mapping $\theta \mapsto F(\Omega_\theta)$, from $W^{1,\infty}(\mathbb{R}^d, \mathbb{R}^d)$ into $\mathbb{R}$, is Fréchet differentiable at $\theta = 0$; the corresponding derivative is denoted by $F'(\Omega)(\theta)$. In practice, the deformations θ featured in this definition are restrained to a subset of $W^{1,\infty}(\mathbb{R}^d, \mathbb{R}^d)$; in the following, we shall consider the sets

$$\Theta^k = \left\{ \theta \in \mathcal{C}^{k,\infty}(\mathbb{R}^d, \mathbb{R}^d), \ \theta = 0 \text{ on } \Gamma_D \cup \Gamma_N \cup \Gamma_0 \right\},$$

where $k \geq 1$, and $\mathcal{C}^{k,\infty}(\mathbb{R}^d, \mathbb{R}^d)$ is the set of k times continuously differentiable functions from $\mathbb{R}^d$ into itself, whose derivatives up to order k are uniformly bounded.
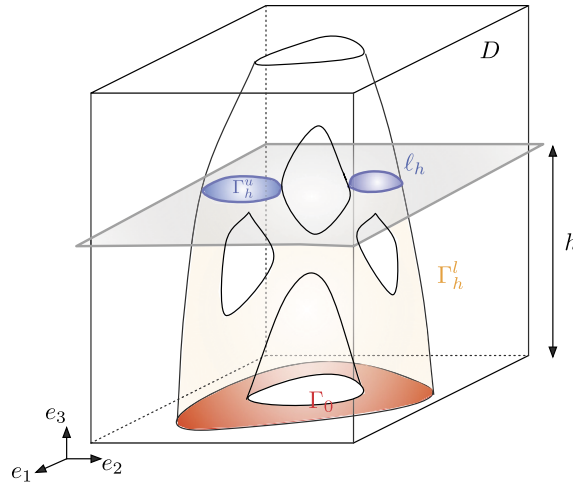
Fig. 2. Intermediate shape Ω_h at height h during the construction of the final structure Ω: the red zone is the lower boundary Γ_0 and the blue zone is the upper boundary Γ_h^u.

For instance, if f is smooth, it is well known (see [3]) that the objective (2) is shape differentiable when deformations are restrained to Θ^k, $k \geq 1$, and that its shape derivative reads:

$$\forall \theta \in \Theta^k, \quad J'(\Omega)(\theta) = -\int_\Gamma Ae(u_\Omega^m) : e(u_\Omega^m)\, \theta \cdot n\, \mathrm{d}s.$$

3. Description and analysis of the mechanical constraint

In this section, we introduce and analyze mathematically our new mechanical constraint functional $P(\Omega)$ describing the manufacturing process of shapes.

3.1. Formulation of the constraint functional $P(\Omega)$

The constraint $P(\Omega)$ relies on the mechanical situation of Ω in the course of the manufacturing process: assuming a vertical build direction e_d (the dth vector of the canonical basis $(e_1, ..., e_d)$ of $\mathbb{R}^d$), Ω is enclosed in a box $D = S \times (0, H)$, where $S \subset \mathbb{R}^{d-1}$. In practice, D represents the build chamber. For $h \in (0, H)$,

$$\Omega_h := \Omega \cap \left\{ x = (x_1, ..., x_d) \in \mathbb{R}^d, \ 0 < x_d < h \right\} \tag{4}$$

is the *intermediate shape* describing the stage where the *final shape* Ω is assembled up to height h. The boundary $\partial \Omega_h$ is decomposed in a different fashion from that of Section 2:

$$\partial \Omega_h = \Gamma_0 \cup \Gamma_h^u \cup \Gamma_h^l, \text{ where }$$
- $\Gamma_0 = \{x \in \partial \Omega_h, \ x_d = 0\}$ is the contact region between Ω and the build table,
- $\Gamma_h^u = \{x \in \partial \Omega_h, \ x_d = h\}$ is the upper side of the intermediate structure,
- $\Gamma_h^l = \partial \Omega_h \setminus (\overline{\Gamma_0} \cup \overline{\Gamma_h^u})$ is the lateral surface.

Eventually, we define $\ell_h := \{x \in \partial \Omega, \ x_d = h\}$, the part of the boundary $\partial \Omega$ lying at height h (typically a curve in three space dimensions); see Fig. 2 about these notations.

Each intermediate shape Ω_h is clamped on Γ_0, and is only subjected to gravity effects, accounted for by a body force $g \in L^2(\mathbb{R}^d)^d$. Its elastic displacement $u_{\Omega_h}^c \in H_{\Gamma_0}^1(\Omega_h)^d$ satisfies the system:

$$\begin{cases} -\mathrm{div}(Ae(u_{\Omega_h}^c)) = g & \text{in } \Omega_h, \\ u_{\Omega_h}^c = 0 & \text{on } \Gamma_0, \\ Ae(u_{\Omega_h}^c)n = 0 & \text{on } \Gamma_h^l \cup \Gamma_h^u, \end{cases} \tag{5}$$

The compliance c_{Ω_h} of Ω_h then reads:

$$c_{\Omega_h} = \int_{\Omega_h} Ae(u_{\Omega_h}^c) : e(u_{\Omega_h}^c)\, \mathrm{d}x = \int_{\Omega_h} g \cdot u_{\Omega_h}^c\, \mathrm{d}x. \tag{6}$$

Our constraint $P(\Omega)$ of the *final structure* Ω aggregates the compliances of all the *intermediate shapes*:

$$P(\Omega) = \int_0^H j(c_{\Omega_h}) \, \mathrm{d}h, \tag{7}$$

where $j : \mathbb{R} \to \mathbb{R}$ is a given, smooth function. For instance, using $j(s) = s^p$ for $1 \le p < \infty$ (and elevating (7) to the power $1/p$), $P(\Omega)$ is the $L^p(0, H)$ norm of the mapping $h \mapsto c_{\Omega_h}$. Recall that a close approximation of the L^∞ norm functional $\Omega \mapsto \sup_{h \in (0, H)} |c_{\Omega_h}|$ is classically achieved by high values of the exponent p.

Note that, as pointed out in the introduction, $P(\Omega)$ only involves the intermediate stages Ω_h of the construction of Ω where the successive layers are completed (and not all the stages where these layers are themselves under construction, and partially assembled).

Remark 1. We considered gravity forces in (5) and compliance in (6): other choices are of course possible and are minor variants of our approach. More generally, it is only incidental that similar mechanical models (namely, linear elasticity systems) are used for describing the mechanical and manufacturing stages of shapes. One could very well imagine modeling cooling effects with a constraint involving the temperature of the intermediate shapes Ω_h via the heat equation; see the forthcoming article [2] about this idea.

3.2. Differentiability of $P(\Omega)$ with respect to the domain

Throughout this section, we consider a fixed shape $\Omega \in \mathcal{U}_{\mathrm{ad}}$. The rigorous exposition of the shape differentiability analysis of $P(\Omega)$ requires that we introduce two open sets $\mathcal{O}_1 \Subset \mathcal{O}_2$ in $\mathbb{R}^d$ and a smooth function $\chi : \mathbb{R}^d \to \mathbb{R}$ such that:

$$\left\{ x \in \partial\Omega \setminus \overline{\Gamma_0}, \; n(x) \cdot e_d = \pm 1 \right\} \subset \mathcal{O}_1, \; 0 \le \chi \le 1, \; \chi \equiv 0 \text{ on } \mathcal{O}_1, \text{ and } \chi \equiv 1 \text{ on } \mathbb{R}^d \setminus \overline{\mathcal{O}_2}.$$

In other words, $\mathcal{O}_1$ is an open neighborhood of the 'flat horizontal regions' of $\partial\Omega \setminus \overline{\Gamma_0}$, and χ is a cutoff function whereby these regions will be ignored. Using these notations, the relevant sets for deformations of Ω are the Banach spaces

$$X^k = \left\{ \theta = \chi\widetilde{\theta}, \; \widetilde{\theta} \in \Theta^k \right\}, \text{ equipped with the quotient norm } ||\theta||_{X^k} = \inf\left\{ ||\widetilde{\theta}||_{C^{k,\infty}(\mathbb{R}^d, \mathbb{R}^d)}, \; \theta = \chi\widetilde{\theta} \right\}. \tag{8}$$

Among other things, vector fields $\theta \in X^k$ vanish near the points of $\partial\Omega \setminus \overline{\Gamma_0}$ where the normal vector n is parallel to e_d.

Let us explain the roles of the cutoff function χ and of the space X^k of shape perturbations:

– deformations Ω_θ of Ω, with $\theta \in X^k$, can be equivalently described by 'horizontal' perturbations (see Proposition 3.2), which are the only ones for which the shape derivative of the compliances c_{Ω_h} can be rigorously calculated owing to Lemma 3.2;
– deformations $\theta \in X^k$ vanish around any point $x \in \partial\Omega$ where $n(x)$ is 'vertical'. This is because at such points x (where the tangent plane is 'horizontal') the intermediate structure Ω_h at height $h = x_d$ shows a turning point at x, and therefore may be not even Lipschitz regular around x. The poor regularity of $u^c_{\Omega_h}$ in this region (see [13] §3.3 for a related study) would be an obstruction to our mathematical analysis.

The main result of this section is the following:

Theorem 3.1. *The functional $P(\Omega)$ given by (7) is shape differentiable at Ω, in the sense that the mapping $\theta \mapsto P(\Omega_\theta)$, from X^k into $\mathbb{R}$ is differentiable for $k \ge 1$. Its derivative is:*

$$\forall \theta \in X^k, \; P'(\Omega)(\theta) = \int_{\partial\Omega \setminus \overline{\Gamma_0}} \mathcal{D}_\Omega \, \theta \cdot n \, \mathrm{d}s, \tag{9}$$

where the integrand factor $\mathcal{D}_\Omega$ is defined, for a.e. $x \in \partial\Omega \setminus \overline{\Gamma_0}$, by:

$$\mathcal{D}_\Omega(x) = \int_{x_d}^H j'(c_{\Omega_h}) \left(2g \cdot u^c_{\Omega_h} - Ae(u^c_{\Omega_h}) : e(u^c_{\Omega_h}) \right)(x) \, \mathrm{d}h. \tag{10}$$

The shape sensitivity $P(\Omega)$ expressed in Theorem 3.1 does not result so easily from standard arguments, since $P(\Omega)$ involves all the intermediate structures Ω_h of Ω, which are only Lipschitz regular (in particular, they show angles at the tip of the upper boundary). We perform the proof in several steps.

(1) In Section 3.2.1, we start by proving that $\theta \mapsto P(\Omega_\theta)$ is differentiable if θ is restricted to the subset

$$X_H^k := \left\{ \theta \in X^k, \ \theta \cdot e_d = 0 \right\}$$

of 'horizontal' perturbations in X^k, and we show that formulae (9), (10) hold in this case.

(2) We prove in Section 3.2.2 that for a given $\theta \in X^k$, there exists a horizontal deformation $\xi \equiv \xi(\theta) \in X_H^k$ accounting for the same perturbed shape: $\Omega_\theta = \Omega_{\xi(\theta)}$. We also prove that the mapping $\theta \mapsto \xi(\theta)$ is differentiable, and we calculate its derivative.

(3) Theorem 3.1 arises in Section 3.2.3 as a consequence of chain rule and of the two previous points.

Remark 2. Formulae (9) and (10) have an intuitive structure: the shape gradient of $P(\Omega)$ at a point $x = (x_1, ..., x_d) \in \partial\Omega \setminus \overline{\Gamma_0}$ involves the elastic energy in x for all the intermediate structures Ω_h, $h > x_d$.

3.2.1. Step 1: shape differentiability of $\theta \mapsto P(\Omega_\theta)$ when $\theta \in X_H^k$

Let us start with the following lemma:

Lemma 3.2. *The compliance $\theta \mapsto c_{(\Omega_\theta)_h}$ at level h, defined by (6), is Fréchet differentiable over X_H^k for $k \geq 1$, and the corresponding derivative reads:*

$$\forall \theta \in X_H^k, \ c'_{\Omega_h}(\theta) = \int_{\Gamma_h^l} \left(2g \cdot u_{\Omega_h}^c - Ae(u_{\Omega_h}^c) : e(u_{\Omega_h}^c) \right) \theta \cdot n \, ds. \tag{11}$$

Proof. The key feature of horizontal deformations lies in the following relation, which holds for $\theta \in X_H^k$ small enough:

$$(\Omega_\theta)_h = \{ x \in \Omega_\theta, \ 0 < x_d < h \} \equiv (\Omega_h)_\theta = (\mathrm{Id} + \theta)(\Omega_h).$$

Hence, because it only involves deformations $\theta \in X_H^k$, Lemma 3.2 merely boils down to the differentiation of the compliance $\Omega \mapsto c_\Omega$ defined by (6) at $\Omega = \Omega_h$. The only difference with the usual setting, as in, e.g., [3,15], is that the domain Ω_h is not smooth. More precisely, Ω_h is piecewise smooth and exhibits corners in two dimensions, ridge edges in three dimensions, at points $x \in \ell_h$ (see again Fig. 2).

However, Ω_h is necessarily locally convex around the sharp features formed by the points $x \in \ell_h$ where the normal vector $n(x)$ is not parallel to e_d (in two dimensions, the angles corresponding to these corners are in $(0, \pi)$). As a consequence, the theory of elliptic equations in polygonal domains implies that the solution $u_{\Omega_h}^c$ to (5) enjoys H^2 regularity in $\Omega_h \setminus \overline{\mathcal{O}_1}$ (see [13], Remark 3.2.4.6).

Since deformations $\theta \in X^k$ (in particular $\theta \in X_H^k$) identically vanish on $\mathcal{O}_1$, which contains the 'bad points' where $n(x)$ is parallel to e_d (see (8)), the classical arguments (see [15], §5.3) leading to the expression (11) for the shape derivative of $\Omega \mapsto c_\Omega$ at Ω_h, involving the calculation of the Lagrangian and Eulerian derivatives of the mapping $\Omega \mapsto u_\Omega^c$ at Ω_h, and elementary (but tedious) calculations based on the Green formula, can be worked out in our particular situation. Similar calculations are performed in a slightly more general context in Proposition 4.2 below, and we do not replicate the argument. $\square$

We are now in good shape for proving Theorem 3.1 in the special case where $\theta \in X_H^k$.

Proposition 3.1. *The mapping $\theta \mapsto P(\Omega_\theta)$ defined by (7), from X_H^k into $\mathbb{R}$ (for $k \geq 1$), is Fréchet differentiable at $\theta = 0$. Its shape derivative reads:*

$$\forall \theta \in X_H^k, \ P'(\Omega)(\theta) = \int_{\partial\Omega \setminus \overline{\Gamma_0}} \mathcal{D}_\Omega \, \theta \cdot n \, ds, \ \text{where } \mathcal{D}_\Omega \text{ is given by (10).}$$

Proof. Let us first discuss the shape differentiability of $P(\Omega)$; denoting by $m(\theta, h) = j(c_{(\Omega_h)_\theta})$, it follows from Lemma 3.2 (and arguments similar to those involved in its proof) that:

– the mapping $(\theta, h) \mapsto m(\theta, h)$ is continuous on $\mathcal{X} \times (0, H)$, where $\mathcal{X}$ is a neighborhood of 0 in X_H^k;
– for any $h \in (0, H)$, the mapping $\theta \mapsto m(\theta, h)$ is Fréchet differentiable on $\mathcal{X}$;
– the (partial) Fréchet derivative $(\theta, h) \mapsto \frac{\partial m}{\partial \theta}(\theta, h)$ of $\theta \mapsto m(\theta, h)$ is continuous from $\mathcal{X} \times (0, H)$ into the dual space of X_H^k.

Then, it follows from the Lebesgue dominated convergence theorem and Lemma 3.2 that $\theta \mapsto P(\Omega_\theta)$ is Fréchet differentiable at $\theta = 0$, and that its derivative reads:

$$\forall \theta \in X_H^k, \quad P'(\Omega)(\theta) = \int_0^H j'(c_{\Omega_h})\, c_{\Omega_h}'(\theta)\, \mathrm{d}h.$$

Recalling the expression (11) of $c_{\Omega_h}'(\theta)$ and using the shorthand $I(x,h) \equiv (2g \cdot u_{\Omega_h}^c - Ae(u_{\Omega_h}^c) : e(u_{\Omega_h}^c))(x)$, this rewrites:

$$P'(\Omega)(\theta) = \int_0^H j'(c_{\Omega_h}) \left(\int_{\Gamma_h^l} I(x,h)(\theta \cdot n)(x)\, \mathrm{d}s(x) \right) \mathrm{d}h. \tag{12}$$

The rest of the proof relies on repeated applications of the Fubini theorem, which in particular entails:

$$\int_{\Gamma_h^l} \rho(x)\, \mathrm{d}x = \int_0^h \int_{\ell_z} \rho(x)\, \mathrm{d}\ell(x)\, \mathrm{d}z,$$

for a (smooth) function ρ. From (12), we obtain successively:

$$
\begin{aligned}
P'(\Omega)(\theta) &= \int_0^H \int_0^h \int_{\ell_z} j'(c_{\Omega_h}) I(x,h)(\theta \cdot n)(x)\, \mathrm{d}\ell(x)\, \mathrm{d}z\, \mathrm{d}h \\
&= \int_0^H \int_z^H \int_{\ell_z} j'(c_{\Omega_h}) I(x,h)(\theta \cdot n)(x)\, \mathrm{d}\ell(x)\, \mathrm{d}h\, \mathrm{d}z \\
&= \int_0^H \int_{\ell_z} \left(\int_{x_d}^H j'(c_{\Omega_h}) I(x,h)\, \mathrm{d}h \right) (\theta \cdot n)(x)\, \mathrm{d}\ell(x)\, \mathrm{d}z \\
&= \int_{\partial\Omega \setminus \overline{\Gamma_0}} \left(\int_{x_d}^H j'(c_{\Omega_h}) I(x,h)\, \mathrm{d}h \right) (\theta \cdot n)(x)\, \mathrm{d}s(x),
\end{aligned}
$$

which is the desired conclusion. $\square$

3.2.2. Step 2: parameterization by horizontal perturbations

In this section, we prove that 'horizontal' perturbations $\theta \in X_H^k$ are the only needed ingredient to describe variations of Ω of the form Ω_θ, at least when $\theta \in X^k$ (here again, the cutoff function χ plays a key role). For this purpose, it is convenient to introduce an alternative way to express identities of the form $\Omega_\theta = \Omega_\xi$, for $\theta, \xi \in X^k$. Let us consider an implicit representation for Ω, that is, a smooth function $\phi : \mathbb{R}^d \to \mathbb{R}$ such that:

$$
\begin{cases}
\phi(x) < 0 & \text{if } x \in \Omega, \\
\phi(x) = 0 & \text{if } x \in \partial\Omega, \\
\phi(x) > 0 & \text{if } x \in \mathbb{R}^d \setminus \overline{\Omega}.
\end{cases}
\tag{13}
$$

For arbitrary vector fields $\theta, \xi \in W^{1,\infty}(\mathbb{R}^d, \mathbb{R}^d)$ with $||\theta||_{W^{1,\infty}(\mathbb{R}^d, \mathbb{R}^d)} < 1$, $||\xi||_{W^{1,\infty}(\mathbb{R}^d, \mathbb{R}^d)} < 1$, we define

$$\mathcal{F}(\theta, \xi) = \phi \circ (\mathrm{Id} + \theta)^{-1} \circ (\mathrm{Id} + \xi)$$

as an element in the set $\mathcal{C}(\partial\Omega)$ of continuous functions on $\partial\Omega$.

Lemma 3.3. *Let $\theta, \xi \in W^{1,\infty}(\mathbb{R}^d, \mathbb{R}^d)$ be such that*

$$||\theta||_{W^{1,\infty}(\mathbb{R}^d, \mathbb{R}^d)} < 1, \text{ and } ||\xi||_{W^{1,\infty}(\mathbb{R}^d, \mathbb{R}^d)} < 1. \tag{14}$$

Then the domains Ω_θ and Ω_ξ coincide if and only if $\mathcal{F}(\theta, \xi) = 0$ in $\mathcal{C}(\partial\Omega)$.

Proof. We only need to discuss the 'if' part of the above statement: assume that $\mathcal{F}(\theta, \xi) = 0$. Because of (14), Ω_θ and Ω_ξ are bounded, Lipschitz regular domains that are Lipschitz diffeomorphic, see [10]. For the same reason, $\partial\Omega_\theta$ and $\partial\Omega_\xi$ are compact, Lipschitz submanifolds of $\mathbb{R}^d$ that are also Lipschitz diffeomorphic.
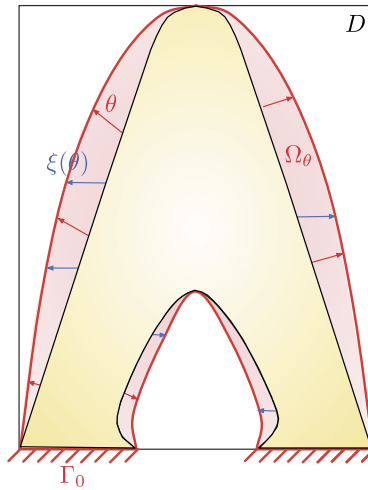
Fig. 3. Perturbation of a two-dimensional shape Ω by a vector field $\theta \in X^k$, and by the corresponding horizontal deformation $\xi(\theta) \in X_H^k$.

Moreover, since the function $\phi \circ (\mathrm{Id} + \theta)^{-1}$ implicitly describes Ω_θ (in the sense that (13) holds with Ω_θ instead of Ω), and since $\mathcal{F}(\theta, \xi) = 0$ implies that $\phi \circ (\mathrm{Id} + \theta)^{-1}$ vanishes on $(\mathrm{Id} + \xi)(\partial\Omega) = \partial\Omega_\xi$, if follows that $\partial\Omega_\xi \subset \partial\Omega_\theta$.

Let us now write $\partial\Omega_\xi = \bigcup_{i=1}^N \mathcal{B}_i$ as the disjoint reunion of its connected components; each $\mathcal{B}_i$ is a compact, Lipschitz submanifold in $\mathbb{R}^d$, and so it is a connected component of $\partial\Omega_\theta$ too. Hence, if the inclusion $\partial\Omega_\xi \subset \partial\Omega_\theta$ were strict, there would exist one Lipschitz submanifold $\mathcal{B} \subset \mathbb{R}^d$, disjoint from $\partial\Omega_\xi$, such that $\partial\Omega_\theta = \mathcal{B} \cup \partial\Omega_\xi$, in contradiction with the fact that $\partial\Omega_\theta$ and $\partial\Omega_\xi$ are Lipschitz diffeomorphic. $\quad\square$

Before proceeding, let us introduce an additional notation: when $x \in \partial\Omega$, $n_H(x) := n(x) - (n(x) \cdot e_d)e_d$ denotes the orthogonal projection of the normal vector to Ω on the 'horizontal space', spanned by $e_1, ..., e_{d-1}$.

Recall (see [15], Prop. 5.4.14) that the normal vector field n can be extended from $\partial\Omega$ to $\mathbb{R}^d$ as a whole, into a vector field of class $\mathcal{C}^\infty$ that has unit norm in a neighborhood of $\partial\Omega$. In the following, with a small abuse of notations, we still denote by n (resp. n_H) this extended normal vector field (resp. its projection on the horizontal space).

The desired result is the following; see Fig. 3 for an illustration.

Proposition 3.2. *For every $k \geq 1$, there exists a mapping $\theta \mapsto \xi(\theta)$, from a neighborhood $\mathcal{X}$ of 0 in X^{k+1} into X_H^k such that, for $\theta \in \mathcal{X}$, Ω_θ and $\Omega_{\xi(\theta)}$ coincide.*

In addition, $\theta \mapsto \xi(\theta)$ is Fréchet differentiable on $\mathcal{X}$ and the restriction to $\partial\Omega$ of its derivative at $\theta = 0$ reads:

$$\forall \theta \in X^{k+1}, \ \xi'(0)(\theta)\Big|_{\partial\Omega} = \frac{1}{|n_H|^2}(\theta \cdot n)\, n_H. \tag{15}$$

Proof. The proof is decomposed into three steps.

(i): Let us define the Banach spaces

$$\mathcal{F}^k = \left\{ \zeta \in \mathcal{C}^k(\partial\Omega), \ \zeta = 0 \text{ on } \Gamma_0 \cup \Gamma_D \cup \Gamma_N \right\},$$

and

$$Y^k = \left\{ \zeta = \chi\widetilde{\zeta}, \ \widetilde{\zeta} \in \mathcal{F}^k \right\}, \text{ equipped with the norm } ||\zeta||_{Y^k} = \inf\left\{ ||\widetilde{\zeta}||_{\mathcal{C}^k(\partial\Omega)}, \ \widetilde{\zeta} \in \mathcal{F}^k \text{ s.t. } \zeta = \chi\widetilde{\zeta} \right\}. \tag{16}$$

Introducing a sufficiently small neighborhood $\mathcal{X}$ (resp. $\mathcal{Y}$) of 0 in X^{k+1} (resp. in Y^k), let us define:

$$\forall \theta \in \mathcal{X}, \ \forall \zeta \in \mathcal{Y}, \ \mathcal{G}(\theta, \zeta) = \phi \circ (\mathrm{Id} + \theta)^{-1} \circ (\mathrm{Id} + \zeta n_H) \in \mathcal{C}^k(\partial\Omega). \tag{17}$$

Our first observation is that $\mathcal{G}$ actually maps $\mathcal{X} \times \mathcal{Y}$ into Y^k. Indeed, if $\theta \in \mathcal{X}$ and $\zeta \in \mathcal{Y}$, there exist $\widetilde{\theta} \in \Theta^k$ and $\widetilde{\zeta} \in \mathcal{F}^k$ such that $\theta = \chi\widetilde{\theta}$ and $\zeta = \chi\widetilde{\zeta}$. Then, for $x \in \partial\Omega$, letting $z = (\mathrm{Id} + \zeta n_H)(x)$, we first calculate:

$$(\mathrm{Id} + \theta)^{-1}(z) - z = (\mathrm{Id} + \theta)^{-1}(z) - (\mathrm{Id} + \theta)^{-1}(z + \theta(z)),$$

$$= \chi(z) \int_0^1 \nabla((\mathrm{Id} + \theta)^{-1})(z + t\theta(z))\, \widetilde{\theta}(z)\, \mathrm{d}t. \tag{18}$$

Using Taylor's formula on $\chi(z)$ in the right-hand side of the above formula yields:

$$\chi(z) = \chi(x) + \chi(x)\widetilde{\zeta}(x) \int_0^1 \nabla\chi(x + t\zeta(x)n_H(x)) \cdot n_H(x) \, dt.$$

It follows that there exists $r \in \Theta^k$ such that:

$$(\mathrm{Id} + \theta)^{-1} \circ (\mathrm{Id} + \zeta n_H) = \mathrm{Id} + \chi r.$$

Then, for arbitrary $x \in \partial\Omega$, we obtain:

$$
\begin{aligned}
\mathcal{G}(\theta, \zeta)(x) = (\phi \circ (\mathrm{Id} + \theta)^{-1}(\mathrm{Id} + \zeta n_H))(x) &= \phi(x + \chi(x)r(x)) - \phi(x), \\
&= \chi(x) \int_0^1 \nabla\phi(x + t\chi(x)r(x)) \cdot r(x) \, dt,
\end{aligned}
$$

which confirms that $\mathcal{G}(\theta, \zeta) \in Y^k$.

(ii): Using analogous arguments, it is easily seen that $\mathcal{G}$ is differentiable; its partial differential at $(0,0)$ with respect to the ζ variable reads:

$$\forall \widehat{\zeta} \in Y^k, \quad d_\zeta \mathcal{G}(0,0)(\widehat{\zeta}) = (\nabla\phi \cdot n_H)\widehat{\zeta} = |n_H|^2 \widehat{\zeta}. \tag{19}$$

Since the partial differential $d_\zeta \mathcal{G}(0,0)$ defined by (19) is invertible from Y^k into itself, the Implicit Function theorem (see, e.g., [16], Chapter I, Theorem 5.9) allows us to conclude that, after possibly taking smaller neighborhoods $\mathcal{X}$ and $\mathcal{Y}$ of 0 in X^{k+1} and Y^k respectively, there exists a mapping $\mathcal{X} \ni \theta \mapsto \zeta(\theta) \in \mathcal{Y}$ of class $\mathcal{C}^1$ such that:

$$\forall \theta \in \mathcal{X}, \ \zeta \in \mathcal{Y}, \ \mathcal{G}(\theta, \zeta) = 0 \Leftrightarrow \zeta = \zeta(\theta).$$

(iii): At this point, the only remaining operation is to extend the scalar function $\zeta(\theta) : \partial\Omega \to \mathbb{R}$ into a vector field defined on $\mathbb{R}^d$ as a whole. To this end, we denote by $p_{\partial\Omega}(x)$ the closest point on $\partial\Omega$ to an arbitrary point $x \in \mathbb{R}^d$; since $\partial\Omega$ is smooth, $x \mapsto p_{\partial\Omega}(x)$ is well defined and smooth on a tubular neighborhood $\mathcal{V}$ of $\partial\Omega$; see again [15], Prop. 5.4.14. Let also $\gamma : \mathbb{R}^d \to \mathbb{R}^d$ be a smooth function such that $\gamma \equiv 1$ on a smaller neighborhood of $\partial\Omega$ and $\gamma \equiv 0$ on $\mathbb{R}^d \setminus \overline{\mathcal{V}}$. We now define, for $\theta \in \mathcal{X}$,

$$\xi(\theta) = (\zeta(\theta) \circ p_{\partial\Omega}) \, \gamma n_H \in X^k.$$

It readily follows from Lemma 3.3 that $\Omega_\theta = \Omega_{\xi(\theta)}$. Eventually, differentiating the relation $\mathcal{G}(\theta, \zeta(\theta)) = 0$ with respect to θ, then evaluating at $\theta = 0$, we obtain the Fréchet derivative of $\theta \mapsto \zeta(\theta)$ at $\theta = 0$:

$$\forall \theta \in X^{k+1}, \ \zeta'(0)(\theta) = \frac{1}{|n_H|^2} \theta \cdot n,$$

which readily leads to (15) and terminates the proof. □

Remark 3. Notice that the horizontal deformation $\xi(\theta)$ supplied by Proposition 3.2, giving rise to the same variation Ω_θ of Ω as the argument θ, has one degree of regularity less than θ. This technical point is a side effect of our application of the Implicit Function theorem to the function $\mathcal{G}$ defined by (17) and of the underlying choice (16) of functional spaces (see in particular formula (18), where we need one more derivative for θ). We do not know whether this result can be improved.

3.2.3. End of the proof of Theorem 3.1

For $k \geq 1$, let $\theta \mapsto \xi(\theta)$ be the mapping from X^{k+1} into X_H^k supplied by Proposition 3.2. Then, as a consequence of definitions, it holds, for $\theta \in X^{k+1}$ small enough that $\Omega_\theta = \Omega_{\xi(\theta)}$ and thus

$$P(\Omega_\theta) = P(\Omega_{\xi(\theta)}).$$

The combination of the chain rule with Proposition 3.1 allows us to conclude.

Remark 4. Formulae (9)–(10) for the shape derivative of $J(\Omega)$ can be retrieved in a formal way by using the interesting results in [23,26], about the differentiation of functions of the form:

$$t \mapsto \int_D (a \circ \Phi_t) \, b \, dx,$$

where a and b are special functions with bounded variations (e.g., characteristic functions), and $t \mapsto \Phi_t$ is the flow generated by a vector field.

Remark 5. A careful investigation of the proof of Theorem 3.1 shows that it was not necessary to assume that the final shape $\Omega \in \mathcal{U}_{\mathrm{ad}}$ is of class $\mathcal{C}^\infty$. Rather a shape of class $\mathcal{C}^{k+1}$ is enough.

4. Practical calculation of the mechanical constraint and of its derivative

The numerical evaluation of $P(\Omega)$ and $P'(\Omega)(\theta)$, or equivalently $\mathcal{D}_\Omega$, by means of formulae (7) and (9), (10) relies on a discretization of the height interval $(0, H)$ with a sequence $0 = h_0 < h_1 < ... < h_N = H$. The intuitive, '0th-order' method to calculate approximations P_N^0 and $\mathcal{D}_N^0$ of $P(\Omega)$ and $\mathcal{D}_\Omega$ consists in replacing c_{Ω_h} and $u_{\Omega_h}^c$ by piecewise constant quantities on each interval $I_i := (h_i, h_{i+1})$ before applying (7) and (10):

$$c_{\Omega_h} \approx c_{\Omega_{h_{i+1}}} \quad \text{and} \quad u_{\Omega_h}^c \approx u_{\Omega_{h_{i+1}}}^c \quad \text{on } \Omega_h, \text{ for } h \in I_i = (h_i, h_{i+1}). \tag{20}$$

This procedure is costly since the piecewise constant approximation (20) is low order: so that its accuracy is guaranteed, the subdivision $\{h_i\}_{i=0,...,N}$ of $(0, H)$ has to be quite fine, which brings about many numerical resolutions of the elasticity system (5) for the $u_{\Omega_{h_i}}^c$.

The efficiency of the '0th-order' method can be improved by constructing a higher-order approximation of the mappings $h \mapsto c_{\Omega_h}$ and $h \mapsto u_{\Omega_h}^c$ on each interval I_i. This requires the calculation of the derivatives of these mappings in an adequate sense, which is the main purpose of this section.

4.1. A review of shape differentiation using diffeomorphisms

This section takes place in a slightly different setting from that of Section 3 where shape derivatives were computed by Hadamard's method, as described in Section 2, i.e. by differentiating functionals of the type $\theta \mapsto F(\Omega_\theta)$. Here, we rather rely on shape variations described by a parameter-dependent diffeomorphism $t \mapsto T_t$. This change in point of views will come in handy in Section 4.2 below: it will allow us to describe intermediate shapes Ω_{h-t} close to Ω_h (see (4) for the definition of Ω_h) as variations of Ω_h, i.e. $\Omega_{h-t} = T_t(\Omega_h)$. This paves the way to a 'natural' notion of differentiation of quantities such as the compliance $h \mapsto c_{\Omega_h}$ defined by (6) and the elastic behavior $h \mapsto u_{\Omega_h}^c$ given by (5) of the intermediate shapes Ω_h with respect to the height parameter.

For the moment, we drop the index h and we consider a bounded domain Ω in $\mathbb{R}^d$, which is only assumed to be Lipschitz regular (as is Ω_h). Its boundary reads as the disjoint reunion $\partial\Omega = \Gamma_0 \cup \Gamma$, where Γ_0 is a non-optimizable subset of $\partial\Omega$ of positive $(d-1)$-dimensional Hausdorff measure.

In this context, we denote by $v_\Omega \in H^1_{\Gamma_0}(\Omega)^d$ the unique solution to the system:

$$\begin{cases} -\mathrm{div}(Ae(v_\Omega)) = g & \text{in } \Omega, \\ Ae(v_\Omega)n = 0 & \text{on } \Gamma, \\ v_\Omega = 0 & \text{on } \Gamma_0, \end{cases}$$

where g is a given function in $H^1(\mathbb{R}^d)^d$. As announced above, the variations of Ω are performed by means of a mapping $t \mapsto T_t$, defined on the interval $(-t_0, t_0)$ for some $t_0 > 0$, which satisfies the properties:

$$\text{for any } t \in (-t_0, t_0), \; T_t \text{ is a diffeomorphism of } \mathbb{R}^d \text{ such that } T_t(\Gamma_0) = \Gamma_0; \tag{21}$$

$$\begin{aligned} &\text{for any } t \in (-t_0, t_0), \; (T_t - \mathrm{Id}) \in W^{1,\infty}(\mathbb{R}^d, \mathbb{R}^d), \text{ and} \\ &\text{the mapping } t \mapsto (T_t - \mathrm{Id}) \text{ is of class } \mathcal{C}^1 \text{ from } (-t_0, t_0) \text{ into } W^{1,\infty}(\mathbb{R}^d, \mathbb{R}^d). \end{aligned} \tag{22}$$

We define $V(x) := \frac{\mathrm{d}T_t(x)}{\mathrm{d}t}|_{t=0} \in W^{1,\infty}(\mathbb{R}^d, \mathbb{R}^d)$.

We now calculate the Eulerian and Lagrangian derivatives of the mapping $\Omega \mapsto v_\Omega$, with respect to variations of Ω driven by T_t. Although the involved arguments are quite classical (see, e.g., [1,21]), the (tedious) proof of these formulae is not so easily found in the literature in the context of the linearized elasticity system. For the sake of convenience, we recall the main steps in the Appendix.

Proposition 4.1. Let $t \mapsto T_t$ be a mapping satisfying (21) and (22). Then,

(i) the mapping $\Omega \mapsto v_\Omega$ has a material derivative in the sense that the transported function $t \mapsto \overline{v_t} := v_{T_t(\Omega)} \circ T_t$, from $(-t_0, t_0)$ into $H^1_{\Gamma_0}(\Omega)^d$ is Fréchet differentiable at $t = 0$; its derivative $\dot{v}_\Omega$ satisfies:

$$\begin{cases} -\mathrm{div}(Ae(\dot{v}_\Omega)) = \mathrm{div}(g \otimes V + (\mathrm{div}V)Ae(v_\Omega) - AC(v_\Omega, V) - Ae(v_\Omega)\nabla V^{\mathrm{T}}) & \text{in } \Omega, \\ Ae(\dot{v}_\Omega)n = -(\mathrm{div}V)Ae(v_\Omega)n + AC(v_\Omega, V)n + Ae(v_\Omega)\nabla V^{\mathrm{T}}n & \text{on } \Gamma \\ \dot{v}_\Omega = 0 & \text{on } \Gamma_0, \end{cases} \tag{23}$$
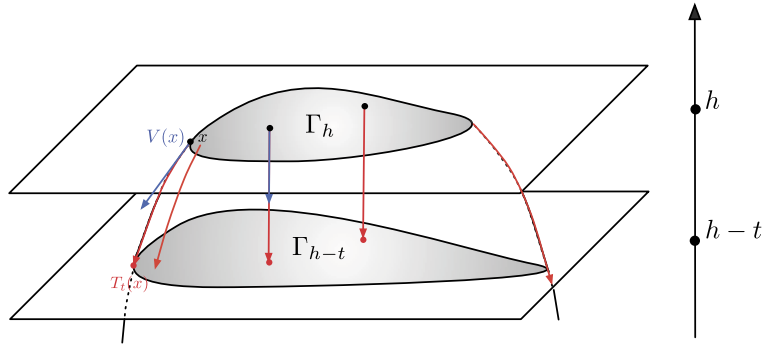
Fig. 4. Example of one diffeomorphism T_t of $\mathbb{R}^d$ mapping Ω_h onto Ω_{h-t}.

where we have used the shorthand:

$$C(v, V) = \frac{1}{2}(\nabla v \nabla V + \nabla V^\mathsf{T} \nabla v^\mathsf{T});$$

(24)

(ii) assuming that $\nabla v_\Omega V \in H^1_{\Gamma_0}(\Omega)^d$, the mapping $\Omega \mapsto v_\Omega$ has an Eulerian derivative $v'_\Omega := \mathring{v}_\Omega - \nabla v_\Omega V$ in $H^1_{\Gamma_0}(\Omega)^d$, where v'_Ω is the solution to the system:

$$\begin{cases} -\mathrm{div}(Ae(v'_\Omega)) = 0 & \text{in } \Omega, \\ Ae(v'_\Omega)n = -\frac{\partial}{\partial n}\left((Ae(v_\Omega)n)\,(V \cdot n) + Ae(v_\Omega)(\nabla_\Gamma(V \cdot n))\right) & \text{on } \Gamma, \\ v'_\Omega = 0 & \text{on } \Gamma_0, \end{cases}$$

(25)

with $\nabla_\Gamma \zeta = \nabla \zeta - (\nabla \zeta \cdot n)n$, the tangential gradient of a (smooth enough) function $\zeta : \Gamma \to \mathbb{R}$.

Remark 6. A word about notations. For (smooth) vector fields $v, w : \mathbb{R}^d \to \mathbb{R}^d$, we denote by ∇v the $d \times d$ Jacobian matrix of v, that is, the matrix with entries: $(\nabla v)_{ij} = \frac{\partial v_i}{\partial x_j}$, $i, j = 1, ..., d$. Accordingly, $\nabla v w$ is the vector field with components $(\nabla v w)_i = (w \cdot \nabla)v_i := \sum_{j=1}^{d} \frac{\partial v_i}{\partial x_j} w_j$.

As an easy consequence, we obtain the following result about the shape differentiation of the *compliance*

$$c_\Omega = \int_\Omega g \cdot v_\Omega \, \mathrm{d}x = \int_\Omega Ae(v_\Omega) : e(v_\Omega) \, \mathrm{d}x.$$

Corollary 4.1. *Let $t \mapsto T_t$ be a mapping satisfying (21) and (22). Then, $t \mapsto c_{T_t(\Omega)}$ is differentiable at $t = 0$, and its derivative reads:*

$$\frac{\mathrm{d}}{\mathrm{d}t}(c_{T_t(\Omega)})\Big|_{t=0} = \int_\Gamma (2g \cdot v_\Omega - Ae(v_\Omega) : e(v_\Omega))\, V \cdot n \, \mathrm{d}s.$$

(26)

4.2. Using shape variations to identify close layers

In this section, we consider a fixed shape $\Omega \in \mathcal{U}_{\mathrm{ad}}$, and a height $h \in (0, H)$ satisfying:

for any $x \in \ell_h$, the normal vector $n(x)$ is not parallel to e_d.

(27)

Our purpose is to show that, for $t > 0$ small enough, the intermediate structures Ω_h and Ω_{h-t} can be expressed in terms of one another via a shape variation of the form (21), (22), namely that there exists a diffeomorphism T_t of $\mathbb{R}^d$ such that $T_t(\Omega_h) = \Omega_{h-t}$ (see Fig. 4). Then we shall use the material in Section 4.1 to differentiate the mappings $h \mapsto c_{\Omega_h}$ and $h \mapsto u^c_{\Omega_h}$; see Section 4.3 below.

Lemma 4.2. *Under the assumption (27), there exist $t_0 > 0$ and a mapping $(-t_0, t_0) \ni t \mapsto T_t$ satisfying (21) and (22), as well as the additional property:*

for $t \in (-t_0, t_0)$, T_t is a diffeomorphism from Ω_h onto Ω_{h-t};

(28)

for any such mapping, let $V \in W^{1,\infty}(\mathbb{R}^d, \mathbb{R}^d)$ be defined by $V(x) = \frac{\mathrm{d}T_t(x)}{\mathrm{d}t}\Big|_{t=0}$. Then,
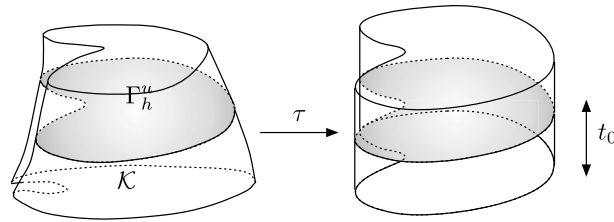
Fig. 5. Illustration of one diffeomorphism τ of $\mathbb{R}^d$ used in the construction of T_t in the proof of Lemma 4.2.

(i) for any point $x \in \Gamma_h^u$, $V(x) \cdot e_d = -1$,
(ii) for any point $x \in \Gamma_0 \cup \Gamma_h^l$, $V(x) \cdot n(x) = 0$.

Proof. First observe that, under the hypothesis (27), the existence of a mapping $t \mapsto T_t$ satisfying (21), (22), and (28) follows from elementary considerations of differential geometry. Indeed, since (27) holds, there exist $t_0 > 0$ and a smooth diffeomorphism τ of $\mathbb{R}^d$ that maps the slice $\mathcal{K} := \{x \in \Omega, \; h - t_0 < x_d < h + t_0\}$ onto the straight cylinder $\Gamma_h^u \times (h - t_0, h + t_0) \subset \mathbb{R}^{d-1} \times \mathbb{R}$ in such a way that:

$$\forall x = (x_1, ..., x_d) \in \mathbb{R}^d, \;\; \pi_d(\tau(x)) = x_d,$$

where $\pi_d : \mathbb{R}^{d-1} \times \mathbb{R} \to \mathbb{R}$ is the standard projection onto the last coordinate: $\pi_d(y, s) = s$ for $y \in \mathbb{R}^{d-1}$ and $y \in \mathbb{R}$; see Fig. 5. Let us now introduce a smooth function $l : (-t_0, t_0) \times \mathbb{R} \to \mathbb{R}$ such that:

– for every $t \in (-t_0, t_0)$, $l(t, \cdot) : \mathbb{R} \to \mathbb{R}$ is a strictly increasing, one-to-one function;
– for $t \in (-t_0, t_0)$, $l(t, s) = s$ for all $s \in (-\infty, h - t_0] \cup [h + t_0, +\infty)$, and $l(t, h) = h - t$.

We finally define:

$$\forall (y, s) \in \mathbb{R}^{d-1} \times \mathbb{R}, \;\; L_t(y, s) = (y, l(t, s)).$$

Then the mapping $T_t = \tau^{-1} \circ L_t \circ \tau$ has the desired properties (21), (22) and (28).

We now turn to the proof of *(i)*. Let $x_0 \in \Gamma_h^u$ be given, and let $\varepsilon > 0$ be so small that the ball $B_\varepsilon(x_0)$ with center x_0 and radius ε is compactly contained in Ω. Let ψ be an arbitrary function of class $\mathcal{C}^\infty$ with compact support in $B_\varepsilon(x_0)$. On the one hand, a change of variables produces:

$$p(t) := \int_{\Omega_{h-t}} \psi(x) \, dx = \int_{\Omega_h} |\det \nabla T_t| \, \psi \circ T_t \, dx,$$

whence, differentiating at $t = 0$ and using Green's formula:

$$p'(0) = \int_{\Omega_h} ((\operatorname{div} V) \psi + \nabla \psi \cdot V) \, dx = \int_{\Gamma_h^u \cap B_\varepsilon(x_0)} \psi \, V \cdot e_d \, ds. \tag{29}$$

On the other hand, since ψ has compact support in $B_\varepsilon(x_0)$, one may alternatively perform the change of variables:

$$p(t) = \int_{\Omega_h} |\det \nabla \widetilde{T}_t| \, \psi \circ \widetilde{T}_t \, dx,$$

where $\widetilde{T}_t$ is the diffeomorphism of $\mathbb{R}^d$ defined by $\widetilde{T}_t(x) = (x_1, x_2, ..., x_{d-1}, x_d - t)$. Hence,

$$p'(0) = \int_{\Gamma_h^u \cap B_\varepsilon(x_0)} \psi \, \widetilde{V} \cdot e_d \, ds, \tag{30}$$

where $\widetilde{V}(x) = \left. \frac{d\widetilde{T}_t(x)}{dt} \right|_{t=0} = -1$. Since both expressions (29) and (30) hold for arbitrary $\psi \in \mathcal{C}_c^\infty(B_\varepsilon(x_0))$, one infers in particular that $V(x) \cdot e_d = -1$, which is the desired result.

The proof of *(ii)* relies on similar arguments. For a given point $x_0 \in \Gamma_h^l \cup \Gamma_0$, take $\varepsilon > 0$ small enough so that the ball $B_\varepsilon(x_0)$ is compactly contained in the half-space $\{x \in \mathbb{R}^d, \, x_d < h\}$. Let also ψ be an arbitrary function of class $\mathcal{C}^\infty$ with compact support in $B_\varepsilon(x_0)$. On the one hand, one has, for $t > 0$ small enough:

$$q(t) := \int_{\Omega_{h-t}} \psi(x) \, dx = \int_{\Omega_h} \psi(x) \, dx, \tag{31}$$

and so $q'(0) = 0$. On the other hand, using the same change of variables as that leading to (29), we obtain:

$$q'(0) = \int_{\Gamma_h^l \cup \Gamma_0} \psi V \cdot n \, ds. \tag{32}$$

Since both expressions (31) and (32) hold for arbitrary ψ, it follows that $(V \cdot n)(x_0) = 0$, and the desired conclusion follows. $\quad\square$

4.3. Derivatives of the mappings $h \mapsto c_{\Omega_h}$ and $h \mapsto u_{\Omega_h}^c$

Our first result is concerned with the derivative of the compliance $h \mapsto c_{\Omega_h}$ defined by (6). The key observation is that, for $t > 0$ small enough, $c_{\Omega_{h-t}} = c_{T_t(\Omega_h)}$, for any mapping $t \mapsto T_t$ furnished by Lemma 4.2. Therefore, combining Corollary 4.1 with Lemma 4.2 straightforwardly yields the following proposition.

Proposition 4.2. *Let $\Omega \in \mathcal{U}_{\mathrm{ad}}$, and $h \in (0, H)$ be such that (27) holds; then the mapping $h \mapsto c_{\Omega_h}$ is differentiable at h and:*

$$\frac{d}{dh}(c_{\Omega_h})\Big|_h = \int_{\Gamma_h^u} (2g \cdot u_{\Omega_h}^c - Ae(u_{\Omega_h}^c) : e(u_{\Omega_h}^c)) \, ds. \tag{33}$$

Let us now turn to giving a suitable meaning to the derivative of $h \mapsto u_{\Omega_h}^c$. Roughly speaking, this derivative is defined as the Eulerian derivative (in the sense of Proposition 4.1) of $t \mapsto u_{T_t(\Omega_h)}^c$, associated with *any* diffeomorphism $t \mapsto T_t$ mapping Ω_h onto Ω_{h-t}.

To make these considerations precise, let us summarize the results from Sections 4.1 and 4.2:

- there exist $t_0 > 0$ and a mapping $(-t_0, t_0) \ni t \mapsto T_t$ satisfying the properties:
  (i) for $t \in (-t_0, t_0)$, T_t is a diffeomorphism of $\mathbb{R}^d$, mapping Ω_h onto Ω_{h-t} such that $T_t(\Gamma_0) = \Gamma_0$,
  (ii) the mapping $(-t_0, t_0) \ni t \mapsto (T_t - \mathrm{Id}) \in W^{1,\infty}(\mathbb{R}^d, \mathbb{R}^d)$ is of class $\mathcal{C}^1$ and we define

$$V(x) := \frac{dT_t(x)}{dt}\Big|_{t=0} \in W^{1,\infty}(\mathbb{R}^d, \mathbb{R}^d); \tag{34}$$

- the mapping $t \mapsto u_{\Omega_{h-t}^c}^c \circ T_t$ is differentiable from $(-t_0, t_0)$ into $H_{\Gamma_0}^1(\Omega_h)^d$. Its derivative Y_{Ω_h} at $t = 0$ may be interpreted as the *Lagrangian derivative* of $h \mapsto u_{\Omega_h^c}$;
- the function $U_{\Omega_h} := Y_{\Omega_h} - \nabla u_{\Omega_h^c} V$ is the solution in $H_{\Gamma_0}^1(\Omega_h)^d$ to the system:

$$\begin{cases} -\mathrm{div}(Ae(U_{\Omega_h})) = 0 & \text{in } \Omega_h, \\ U_{\Omega_h} = 0 & \text{on } \Gamma_0, \\ Ae(U_{\Omega_h})n = 0 & \text{on } \Gamma_h^l, \\ Ae(U_{\Omega_h})n = \frac{\partial}{\partial n}\left((Ae(u_{\Omega_h^c})n)\right) & \text{on } \Gamma_h^u. \end{cases} \tag{35}$$

It is natural to refer to U_{Ω_h} as the *Eulerian derivative* of the mapping $h \mapsto u_{\Omega_h}^c$.

As is clear from (35) (and as expected), U_{Ω_h} is independent of the diffeomorphism $t \mapsto T_t$ used in its construction, as long as T_t satisfies the intuitive properties (34). In particular, U_{Ω_h} does not depend on V since $V(x) \cdot e_d = -1$ for a.e. $x \in \Gamma_h^u$.

Remark 7. Notice that, from a formal point of view, the Eulerian derivative U_{Ω_h} is the derivative of $t \mapsto u_{\Omega_{h-t}}^c$ at $t = 0$, and not that of $t \mapsto u_{\Omega_{h+t}}^c$; the reason for this seemingly unintuitive convention will find proper justification in Section 4.4 (see Formula (37)).

4.4. Practical algorithm

The considerations of Section 4.3 suggest the following procedure for calculating first-order approximations P_N^1 and $\mathcal{D}_N^1$ of $P(\Omega)$ and $\mathcal{D}_\Omega$, respectively. This allows for an accurate and computationally efficient calculation of these quantities, using a coarser subdivision $\{h_i\}_{i=1,\ldots,N}$ of $(0, H)$ than in the calculation of the 0th-order approximate values P_N^0 and $\mathcal{D}_N^0$, defined by (20).
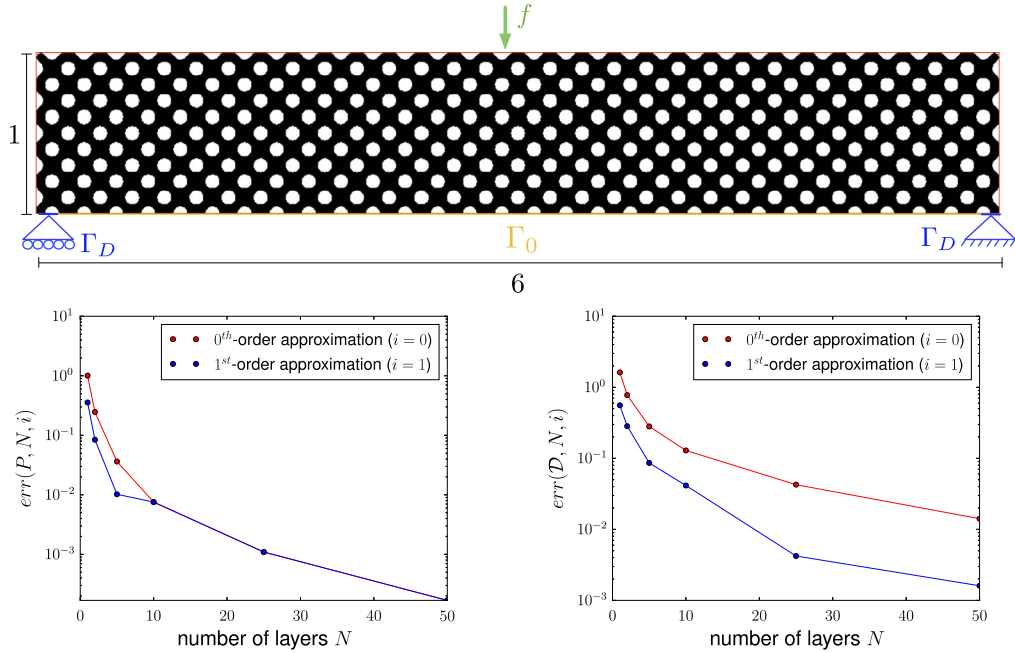
Fig. 6. (Top) Setting of the validation experiment and initial shape Ω_0; (bottom) relative errors of the 0th- and 1st-order approximations of $P(\Omega_0)$ and its derivative $\mathcal{D}_{\Omega_0}$.

(1) For $i = 0, ..., N$ calculate the compliances $c_{\Omega_{h_i}}$ as (6) and the displacements $u^c_{\Omega_{h_i}}$ by solving (5).

(2) For $i = 0, ..., N$, calculate the derivative $\frac{\mathrm{d}}{\mathrm{d}h}(c_{\Omega_h})\big|_{h=h_i}$ of the compliance by using Proposition 4.2.

(3) For $i = 1, ..., N$, calculate the Eulerian derivative $U_{\Omega_{h_i}}$ at h_i by using (35).

(4) On each interval $I_i = (h_i, h_{i+1})$, $i = 0, ..., N-1$, the compliance c_{Ω_h} is approximated by a cubic spline $\widetilde{c}_i(h)$, which is uniquely determined by the data:

$$\widetilde{c}_i(h_i) = c_{\Omega_{h_i}}, \ \ \widetilde{c}_i(h_{i+1}) = c_{\Omega_{h_{i+1}}}, \ \ \widetilde{c}_i{}'(h_i) = \frac{\mathrm{d}}{\mathrm{d}h}(c_{\Omega_h})\Big|_{h_i}, \ \text{and} \ \widetilde{c}_i{}'(h_{i+1}) = \frac{\mathrm{d}}{\mathrm{d}h}(c_{\Omega_h})\Big|_{h_{i+1}}. \tag{36}$$

(5) For $i = 0, ..., N-1$ and $h \in I_i = (h_i, h_{i+1})$, $u^c_{\Omega_h}$ is approximated by $\widetilde{u_h}$, defined by:

$$\widetilde{u_h}(x) = u^c_{\Omega_{h_{i+1}}}(x) + (h_{i+1} - h)\, U_{\Omega_{h_{i+1}}}(x), \ \text{a.e.}\, x \in \Omega_h; \tag{37}$$

notice that the above relation does make sense for $x \in \Omega_h$ regardless of the height $h \in (h_i, h_{i+1})$ since $u^c_{\Omega_{h_{i+1}}}$ and $U_{\Omega_{h_{i+1}}}$ are well defined on $\Omega_h \subset \Omega_{h_{i+1}}$ (see Remark 7).

5. Numerical illustrations

Let us consider the 2d MBB Beam test case: the shapes Ω are contained in a rectangular domain D of size 6×1. Due to symmetry, only half of D is meshed by $300 \times 100 \ \mathbb{Q}_1$ elements. In the context of their final utilization (described by the system (1)), the horizontal displacement of shapes is fixed on a small part of their lower-left side, and both horizontal and vertical displacements are fixed on a small part of its lower-right side, and a unit vertical load $f = (0, -1)$ is applied at the middle of their upper side. When it comes to their construction (modeled by (5)), shapes are built vertically from bottom to top, so that Γ_0 coincides with the lower side of D. The function $j : \mathbb{R} \to \mathbb{R}$ used in the definition (7) of $P(\Omega)$ is simply the identity: $j(s) = s$. The design Ω_0 in Fig. 6 (top) is used for the numerical validation of our methods in Section 5.1 and it is the initial guess for the shape optimization of Section 5.2.

5.1. Validation of the approximations of Section 4

At first, we calculate the functional $P(\Omega)$ and its shape derivative $\mathcal{D}_\Omega$ in the particular case where $\Omega = \Omega_0$, by using a uniform subdivision of $(0, H)$ made of 100 layers and the 0th-order approximation scheme, i.e. we evaluate P^0_{100} and $\mathcal{D}^0_{100}$, which serve as reference values for the comparisons in this section. We then calculate the 0th- and 1st-order approximations
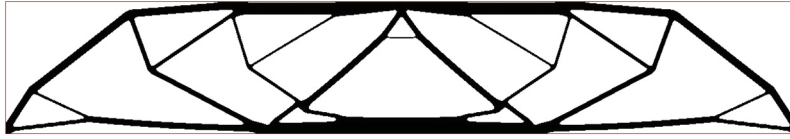
Fig. 7. Optimized design Ω^* for the shape optimization problem (38).
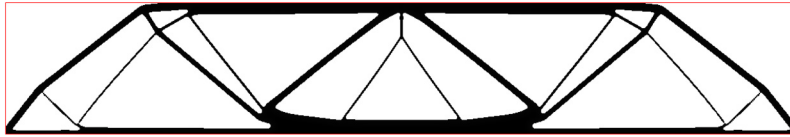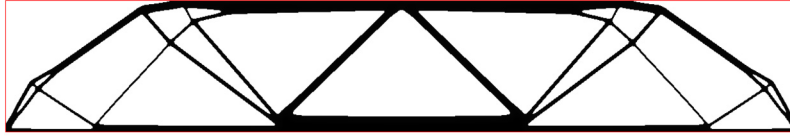

Fig. 8. Optimized shapes for (39) using the respective approximations for $P(\Omega)$ and $\mathcal{D}_\Omega$: (up) P_{100}^0 and $\mathcal{D}_{100}^0$; (down) P_{25}^1 and $\mathcal{D}_{25}^1$.

Table 1
Values of the shape functionals and iteration numbers.

Shape Ω	$J(\Omega)$	$\text{Vol}(\Omega)$	$P(\Omega)$	Iterations	Evaluations
Fig. 7	104.165	0.600	0.730	25	38
Fig. 8 (up)	98.484	0.599	0.343	127	143
Fig. 8 (down)	99.313	0.600	0.343	187	206

P_N^i and $\mathcal{D}_N^i$, $i = 0$ and 1, associated with several subdivisions of $(0, H)$ made of N intervals with equal length. We are interested in the behavior of the relative errors:

$$\text{err}(P, N, i) = \frac{|P_N^i - P_{100}^0|}{P_{100}^0} \quad \text{and} \quad \text{err}(\mathcal{D}, N, i) = \frac{||\mathcal{D}_N^i - \mathcal{D}_{100}^0||_{L^2(\partial\Omega \setminus \overline{\Gamma_0})}}{||\mathcal{D}_{100}^0||_{L^2(\partial\Omega \setminus \overline{\Gamma_0})}}.$$

The results are displayed in Fig. 6 (bottom): while the 1st-order approximation method does not bring a lot of improvement when it comes to evaluating the constraint functional $P(\Omega)$, it allows for a substantial gain (i.e. a faster convergence with respect to the number N of subdivisions) in the evaluation of its derivative.

5.2. A numerical example

Recalling that $J(\Omega)$ is the compliance, defined by (2), we now turn to the shape optimization problem:

$$\min_{\Omega \in \mathcal{U}_{\text{ad}}} J(\Omega) \text{ such that } \text{Vol}(\Omega) \leq 0.2 \, \text{Vol}(D). \tag{38}$$

We first solve (38), starting from the initial design Ω_0, by using an SLP-type algorithm in the spirit of that presented in [9], and the level set method on a fixed Cartesian mesh when it comes to tracking the deformation of shapes [3]. The optimized design Ω^* is shown in Fig. 7; in particular, several overhanging parts appear in Ω^*.

We now add our mechanical constraint $P(\Omega)$ to this problem, and solve:

$$\min_{\Omega \in \mathcal{U}_{\text{ad}}} J(\Omega) \text{ such that } \begin{cases} \text{Vol}(\Omega) \leq 0.2 \, \text{Vol}(D), \\ P(\Omega) \leq 0.5 \, P(\Omega^*). \end{cases} \tag{39}$$

The resulting optimized shapes, obtained by using 0th- and 1st-order approximations of $P(\Omega)$ and $\mathcal{D}_\Omega$ with different (uniform) subdivisions of $(0, H)$ are represented in Fig. 8. The computational effort is significantly different: about 237 h are needed when the 0th-order approximation process is used with $N = 100$ layers, whereas the total calculation takes 'only' 82 h when using 1st-order approximations and $N = 25$ layers. The values of the corresponding quantities of interest are collected in Table 1.

As is clear from the above computational times, the implementation of our algorithm has not been optimized at all. The reasons for such large CPU times are obvious, as are the possible remedies in a near future. Indeed, the optimization algorithm and the Finite Element analyses for the mechanical systems (1) and (5) are carried out in different softwares:

we re-use a previous Scilab script [6] for the optimization algorithm, while we rely on FreeFem++ [14] for the mechanical analyses. Then, the communications between these two softwares is done through file exchanges, a notorious source of unefficiency. Also, we did not investigate the straightforward parallelization of the Finite Element resolutions of all the linear elasticity systems (5) posed on the intermediate structures Ω_h associated with a common shape Ω, which are independent one from another. Our point in giving these CPU data is only to emphasize the improvement in computational efficiency allowed by the use of the 1st-order method instead of the 0th-order one.

Notice that, on the optimized designs in Fig. 8, several overhangs placed at the lower part of the optimal shape Ω^* without manufacturing constraint have vanished. Still, a few overhangs remain in the superior regions of the optimized shapes in Fig. 8; this may be explained in two ways:

– the definition (7) of our mechanical constraint $P(\Omega)$ focuses on the performance (in terms of the self-weight (6)) of the lower intermediate shapes; indeed, high values of the self-weight $c_{\Omega_{h_0}}$ of an intermediate structure Ω_{h_0} generally cause high values of the self-weights c_{Ω_h} of some of the upper intermediate structures Ω_h, $h > h_0$, whereas the converse does not hold;
– The constraint $P(\Omega)$ has been devised under the simplifying assumption that each layer of material is assembled at once, and does not bring into play the stages where these layers are themselves under construction. Hence, completely flat parts such as those observed in the designs of Fig. 8 are not so 'bad' in terms of $P(\Omega)$ as long as they are anchored to the lower structure.

We refer the reader to the companion article [4] for further discussions about the practical use of the mechanical constraint $P(\Omega)$, and variations of it, built upon the same philosophy.

It is also remarkable that the value of the objective function is lower for the constrained problem, meaning that the constraint has the (surprising) effect of driving the algorithm in a lower local minimum (this may be due to the larger number of iterations in the latter case).

Acknowledgements

Appendix A. Proof of Proposition 4.1

Proof of (i). We compute the material or Lagrangian derivative, starting from the variational formulation for $v_{T_t(\Omega)}$:

$$\forall w \in H^1_{\Gamma_0}(T_t(\Omega))^d, \quad \int_{T_t(\Omega)} Ae(v_{T_t(\Omega)}) : e(w) \, \mathrm{d}x = \int_{T_t(\Omega)} g \cdot w \, \mathrm{d}x,$$

which yields, after the usual change of variables, for an arbitrary test function $w \in H^1_{\Gamma_0}(T_t(\Omega))^d$:

$$\int_\Omega |\det \nabla T_t| \, (Ae(v_{T_t(\Omega)}) \circ T_t) : (e(w) \circ T_t) \, \mathrm{d}x = \int_\Omega |\det \nabla T_t|(g \circ T_t) \cdot (w \circ T_t) \, \mathrm{d}x. \tag{A.1}$$

Now, relying on the identities, for any $w \in H^1_{\Gamma_0}(T_t(\Omega))^d$,

$$(\nabla w) \circ T_t = \nabla(w \circ T_t)\nabla T_t^{-1}, \quad e(w) \circ T_t = \frac{1}{2}\left(\nabla(w \circ T_t)\nabla T_t^{-1} + \nabla T_t^{-T}\nabla(w \circ T_t)^T\right),$$

and using test functions of the form $w \circ T_t^{-1}$, $w \in H^1_{\Gamma_0}(\Omega)^d$ in (A.1), we obtain the following variational formulation for $\overline{v_t}$:

$$\forall w \in H^1_{\Gamma_0}(\Omega)^d, \quad \int_\Omega |\det \nabla T_t| \, A\left(\frac{1}{2}\left(\nabla \overline{v_t} \nabla T_t^{-1} + \nabla T_t^{-T}\nabla \overline{v_t}^T\right)\right) : \left(\frac{1}{2}\left(\nabla w \nabla T_t^{-1} + \nabla T_t^{-T}\nabla w^T\right)\right) \, \mathrm{d}x$$

$$= \int_\Omega |\det \nabla T_t|(g \circ T_t) \cdot w \, \mathrm{d}x.$$

At this point, a classical argument using the Implicit Function theorem (see, e.g., [15,20]) reveals that the mapping $t \mapsto \overline{v_t}$ is differentiable, from $(-t_0, t_0)$ into $H^1_{\Gamma_0}(\Omega)^d$ (up to decreasing the value of t_0). Its derivative $\overset{\circ}{v}_\Omega$ at $t = 0$ is the solution to the following variational problem:

$$\forall w \in H^1_{\Gamma_0}(\Omega)^d, \quad \int_\Omega Ae(\mathring{v}_\Omega) : e(w) \, dx = \int_\Omega ((\mathrm{div}V)g \cdot w + \nabla g V \cdot w) \, dx - \int_\Omega (\mathrm{div}V)Ae(v_\Omega) : e(w) \, dx$$

$$+ \int_\Omega (AC(v_\Omega, V) : e(w) + AC(w, V) : e(v_\Omega)) \, dx, \tag{A.2}$$

where $C(v, V)$ is defined by (24), as follows, from a straightforward (yet tedious) calculation. The expression (A.2) can be rearranged owing to the following identities, valid for $w \in H^1_{\Gamma_0}(\Omega)^d$, $g \in H^1(\mathbb{R}^d)^d$, $V \in W^{1,\infty}(\mathbb{R}^d, \mathbb{R}^d)$, and $\sigma \in L^2(\Omega)^{d \times d}$:

$$(\mathrm{div}V)g + \nabla g V = \mathrm{div}(g \otimes V), \text{ and } \sigma : C(w, V) = \frac{1}{2}(\sigma \nabla V^T + \sigma^T \nabla V^T) : \nabla w.$$

It follows from (A.2) that:

$$\forall w \in H^1_{\Gamma_0}(\Omega)^d, \quad \int_\Omega Ae(\mathring{v}_\Omega) : e(w) \, dx = \int_\Omega \mathrm{div}(g \otimes V) \cdot w \, dx - \int_\Omega (\mathrm{div}V)Ae(v_\Omega) : e(w) \, dx$$

$$+ \int_\Omega (AC(v_\Omega, V) : e(w) + (Ae(v_\Omega)\nabla V^T) : \nabla w) \, dx.$$

Eventually, integrating by parts, we end up with the classical formulation (23) for the problem characterizing the material derivative $\mathring{v}_\Omega \in H^1_{\Gamma_0}(\Omega)^d$. □

Proof of (ii). We now consider the Eulerian derivative v'_Ω of v_Ω, defined from $\mathring{v}_\Omega$ via the formula:

$$v'_\Omega = \mathring{v}_\Omega - \nabla v_\Omega V.$$

Using (23), $v'_\Omega \in H^1_{\Gamma_0}(\Omega)^d$ is characterized as the solution to the following problem:

$$\begin{cases} -\mathrm{div}(Ae(v'_\Omega)) = \mathrm{div}(g \otimes V + Ae(\nabla v_\Omega V) + (\mathrm{div}V)Ae(v_\Omega) - AC(v_\Omega, V) - Ae(v_\Omega)\nabla V^T) & \text{in } \Omega, \\ Ae(v'_\Omega)n = -Ae(\nabla v_\Omega V)n - (\mathrm{div}V)Ae(v_\Omega)n + AC(v_\Omega, V)n + Ae(v_\Omega)\nabla V^T n & \text{on } \Gamma, \\ v'_\Omega = 0 & \text{on } \Gamma_D. \end{cases} \tag{A.3}$$

We now simplify (A.3). For $w \in H^1_{\Gamma_0}(\Omega)^d$ and $V \in W^{1,\infty}(\mathbb{R}^d, \mathbb{R}^d)$, the $d \times d$ matrix $\nabla(\nabla w V)$ has entries:

$$(\nabla(\nabla w V))_{ij} = \sum_{k=1}^d \frac{\partial^2 w_i}{\partial x_j \partial x_k} V_k + (\nabla w \nabla V)_{ij}, \quad i, j = 1, ..., d,$$

which produces:

$$Ae(\nabla w V)_{ij} = \sum_{k=1}^d \frac{\partial}{\partial x_k}\left(Ae(w)_{ij}\right) V_k + (AC(w, V))_{ij}. \tag{A.4}$$

Likewise, simple calculations yield:

$$-(\mathrm{div}(Ae(w)) \otimes V)_{ij} = -\sum_{k=1}^d \frac{\partial}{\partial x_k}(Ae(w)_{ik})V_j, \tag{A.5}$$

$$(Ae(w)\nabla V^T)_{ij} = \sum_{k=1}^d Ae(w)_{ik}\frac{\partial V_j}{\partial x_k}, \tag{A.6}$$

and eventually:

$$(\mathrm{div}V)Ae(w)_{ij} = \left(\sum_{k=1}^d \frac{\partial V_k}{\partial x_k}\right) Ae(w)_{ij}. \tag{A.7}$$

Inserting (A.4), (A.5), (A.6) and (A.7) into (A.3), we obtain successively:

$$(g \otimes V + Ae(\nabla v_\Omega V) + (\text{div}V)Ae(v_\Omega) - AC(v_\Omega, V) - Ae(v_\Omega)\nabla V^T)_{ij}$$

$$= \sum_{k=1}^{d} \left(\frac{\partial}{\partial x_k}\left(Ae(v_\Omega)_{ij}\right)V_k + \frac{\partial V_k}{\partial x_k}Ae(v_\Omega)_{ij} - \frac{\partial}{\partial x_k}(Ae(v_\Omega)_{ik})V_j - Ae(v_\Omega)_{ik}\frac{\partial V_j}{\partial x_k} \right),$$

$$= \sum_{k=1}^{d} \left(\frac{\partial}{\partial x_k}\left(Ae(v_\Omega)_{ij}V_k\right) - \frac{\partial}{\partial x_k}(Ae(v_\Omega)_{ik}V_j) \right),$$

whence, as expected,

$$-\text{div}(Ae(v'_\Omega))_i = \sum_{j,k=1}^{d} \frac{\partial^2}{\partial x_j \partial x_k}\left(Ae(v_\Omega)_{ij}V_k - Ae(v_\Omega)_{ik}V_j\right) = 0.$$

Let us now rearrange the boundary condition featured in (A.3). Using again (A.4), (A.6), (A.7), and the fact that $Ae(v_\Omega)n = 0$ on Γ, we obtain the following identity on Γ, for $i = 1, ..., d$:

$$\begin{aligned} (Ae(v'_\Omega)n)_i &= -\sum_{j,k=1}^{d} \frac{\partial}{\partial x_k}(Ae(v_\Omega)_{ij})V_k n_j + \sum_{j=1}^{d} Ae(v_\Omega)_{ij}(\nabla V^T n)_j, \\ &= \sum_{j,k=1}^{d}\left(Ae(v_\Omega)_{ij}\frac{\partial V_k}{\partial x_j}n_k - \frac{\partial}{\partial x_k}(Ae(v_\Omega)_{ij})V_k n_j\right). \end{aligned} \tag{A.8}$$

Now, taking advantage of the fact that $Ae(v_\Omega)n = 0$ on Γ, we infer, by taking derivatives in the direction of a tangential vector field:

$$\sum_{j=1}^{d} \nabla(Ae(v_\Omega)_{ij}) \cdot V_\Gamma\, n_j = \sum_{j=1}^{d} Ae(v_\Omega)_{ij}\nabla n_j \cdot V_\Gamma,$$

where $V_\Gamma = V - (V \cdot n)n$ is the tangential part of the vector field V. Hence (A.8) becomes:

$$\begin{aligned} (Ae(v'_\Omega)n)_i &= -\left(\sum_{j=1}^{d} \frac{\partial}{\partial n}(Ae(v_\Omega)_{ij})n_j\right)(V \cdot n) + \sum_{j=1}^{d} Ae(v_\Omega)_{ij}\left(\sum_{k=1}^{d}\frac{\partial V_k}{\partial x_j}n_k + \nabla n_j \cdot V_\Gamma\right), \\ &= -\frac{\partial}{\partial n}\left((Ae(v_\Omega)n)\right)(V \cdot n) + \sum_{j=1}^{d} Ae(v_\Omega)_{ij}\left(\sum_{k=1}^{d}\frac{\partial}{\partial x_j}(V_k n_k) + \sum_{k=1}^{d}\left(\frac{\partial n_j}{\partial x_k} - \frac{\partial n_k}{\partial x_j}\right)V_k\right). \end{aligned} \tag{A.9}$$

Notice that, in passing from the first to the second line in (A.9), we have used the classical facts from tangential calculus (see [15], Chap. 5):

$$\nabla n = \nabla n^T, \text{ and } \nabla nn = \nabla n^T n = 0 \text{ on a neighborhood of } \partial\Omega.$$

Eventually, using once again these facts together with the boundary condition $Ae(v_\Omega)n = 0$ on Γ, we end up with:

$$Ae(v'_\Omega)n = -\frac{\partial}{\partial n}\left((Ae(v_\Omega)n)\right)(V \cdot n) + Ae(v_\Omega)(\nabla_\Gamma(V \cdot n)) \text{ on } \Gamma,$$

which is the announced result (25). □

References

[1] G. Allaire, Conception optimale de structures, Math. Appl., vol. 58, Springer-Verlag, Berlin, 2007.
[2] G. Allaire, L. Jakabcin, Taking into account thermal residual stresses in topology optimization of structures built by additive manufacturing (in preparation).
[3] G. Allaire, F. Jouve, A.M. Toader, Structural optimization using shape sensitivity analysis and a level-set method, J. Comput. Phys. 194 (2004) 363–393.
[4] G. Allaire, C. Dapogny, R. Estevez, A. Faure, G. Michailidis, Structural optimization under overhang constraints imposed by additive manufacturing technologies (in preparation).
[5] F. Calignano, Design optimization of supports for overhanging structures in aluminum and titanium alloys by selective laser melting, Mater. Des. 64 (2014) 203–213.
[6] S.L. Campbell, J.-P. Chancelier, R. Nikoukhah, Modeling and Simulation in Scilab/Scicos, Springer, New York, 2006.
[7] A. Clausen, Topology Optimization for Additive Manufacturing, Ph.D. Thesis, Technical University of Denmark, 2016.
[8] J. Dumas, J. Hergel, S. Lefebvre, Bridging the gap: automated steady scaffoldings for 3D printing, ACM Trans. Graph. 33 (4) (2014) 1–10.
[9] P. Dunning, H. Kim, Introducing the sequential linear programming level-set method for topology optimization, Struct. Multidiscip. Optim. 51 (2015) 631–643.
[10] L.C. Evans, R.F. Gariepy, Measure Theory and Fine Properties of Functions, CRC Press, Boca Raton, FL, USA, 1992.
[11] A.T. Gaynor, J.K. Guest, Topology optimization considering overhang constraints: eliminating sacrificial support material in additive manufacturing through design, Struct. Multidiscip. Optim. (2016), http://dx.doi.org/10.1007/s00158-016-1551-x.

[12] I. Gibson, D.W. Rosen, B. Stucker, Additive Manufacturing Technology: Rapid Prototyping to Direct Digital Manufacturing, Springer Science Business Media, Inc., 2010.
[13] P. Grisvard, Elliptic Problems in Nonsmooth Domains, Pitman Publishing, Inc., Boston, MA, USA, 1985.
[14] F. Hecht, New development in FreeFem++, J. Numer. Math. 20 (3–4) (2012) 251–265.
[15] A. Henrot, M. Pierre, Variation et optimisation de formes, une analyse géométrique, Math. Appl., vol. 48, Springer, Berlin, 2005.
[16] S. Lang, Fundamentals of Differential Geometry, Springer, 1991.
[17] M. Langelaar, Topology optimization of 3D self-supporting structures for additive manufacturing, Addit. Manuf. 12 (2016) 60–70.
[18] A.M. Mirzendehdel, K. Suresh, Support structure constrained topology optimization for additive manufacturing, Comput. Aided Des. (2016), http://dx.doi.org/10.1016/j.cad.2016.08.006.
[19] K.A. Mumtaz, P. Vora, N. Hopkinson, A method to eliminate anchors/supports from directly laser melted metal powder bed processes, in: Proc. Solid Freeform Fabrication Symposium, Sheffield, UK, 2011, pp. 55–64.
[20] F. Murat, J. Simon, Sur le contrôle par un domaine géométrique, Technical report RR-76015, Laboratoire d'analyse numérique, Paris, 1976.
[21] A. Novotny, J. Sokolowski, Topological Derivatives in Shape Optimization, Springer, Heidelberg, Germany, 2012.
[22] O. Pironneau, Optimal Shape Design for Elliptic Systems, Springer-Verlag, New York, 1984.
[23] F. Santambrogio, F.-X. Vialard, A Semi Derivation Lemma on BV Functions, Technical report, ArXiv Mathematics, 2008.
[24] J. Sokołowski, J.-P. Zolesio, Introduction to Shape Optimization: Shape Sensitivity Analysis, Springer Ser. Comput. Math., vol. 10, Springer, Berlin, 1992.
[25] 3D Systems, Inc., Stereolithography Interface Specification, July 1988.
[26] F.-X. Vialard, Hamiltonian Approach to Geodesic Image Matching, Technical report, ArXiv Mathematics, 2008.